



Modeling the dynamical process of behavioral contagion in human crowds during evacuation

Wenhan Wu ^a, Wenfeng Yi ^b,*

^a Senseable City Laboratory, Massachusetts Institute of Technology, Cambridge, MA 02139, USA

^b College of Artificial Intelligence, China University of Petroleum, Beijing 102249, China

ARTICLE INFO

Keywords:

Behavioral contagion
Evacuation dynamics
Collective behavior
Force-based model
Social influence

ABSTRACT

Behavioral contagion, the process by which individuals adopt behaviors from neighbors, plays a critical role in crowd evacuations by shaping collective decision-making and movement patterns. Despite its observable and tractable nature compared to emotional contagion, however, behavioral contagion remains underexplored in crowd models, with its propagation mechanisms and effects on evacuation dynamics yet to be systematically explored. To address these gaps, we propose a behavioral contagion-based social force model (BC-SFM) that explicitly couples contagion mechanisms with movement behaviors. Numerical simulations show that BC-SFM outperforms the classical SFM by enabling faster and more synchronized changes in escape behaviors, highlighting the performance superiority of our model in characterizing behavioral contagion dynamics. The intensity and heterogeneity of interaction radius and response threshold jointly determine the spatial-temporal dynamics of behavioral contagion, with their effects also varying across different crowd densities. Moreover, four typical contagion mechanisms, shaped by distinct combinations of perceptual capacity and individual responsiveness, significantly affect evacuation dynamics, particularly in terms of efficiency and congestion. These findings demonstrate the pivotal impact of behavioral contagion on emergent evacuation outcomes, offering theoretical foundations for advancing predictive models and adaptive management strategies.

1. Introduction

With the growing size and frequency of mass events in urban environments, understanding collective human behavior during evacuation has become a critical issue in public safety research [1,2]. Over the past decades, substantial progress has been made in modeling pedestrian dynamics [3–5], including many aspects of decision-making [6], route selection [7], and avoidance behavior [8]. These studies have deepened our insights into self-organized phenomena [9] and provided valuable references for the design and optimization of evacuation strategies [10, 11]. As the realism and complexity of simulation techniques increase, researchers have begun to explore higher-order interaction mechanisms, such as decision imitation [12], emotional contagion [13], and spontaneous coordination [14]. Among these, behavioral contagion, the process by which individuals imitate the actions or behaviors of surrounding neighbors, has received increasing attention as an important driver influencing collective behaviors [15,16]. It can trigger synchronized movements, behavioral cascades, or leader-follower structures, all of which significantly reshape the spatio-temporal dynamics of collective motion [17]. However, behavioral contagion, as a potential driver of typical herding behavior, remains insufficiently explored in

crowd modeling. The mechanisms of how local contagion dynamics shape collective behavior shifts during evacuation have yet to be systematically understood.

As a classical microscopic approach, the social force model (SFM) provides a powerful framework to simulate pedestrian motion by modeling self-driven forces, interpersonal interactions, and obstacle avoidance [18,19]. To improve realism, various extensions have been introduced to integrate crucial factors such as visual perception [20,21], individual heterogeneity [22,23], and stress variation [24], which have significantly enhanced the performance of SFM to reproduce complex crowd behaviors and evacuation phenomena. Nevertheless, a universal limitation remains: most SFM-based approaches assume that pedestrians make decisions independently based on predefined physical or cognitive rules, largely ignoring dynamic social influences exerted by surrounding individuals [25]. In fact, pedestrians may adjust their movement behaviors not only according to environmental cues but also in response to the information, actions, or emotional states of nearby neighbors [26,27]. This is especially obvious in emergency situations where local imitation and peer influence can lead to spontaneous behavioral cascades [28]. Therefore, it is important to address this

* Corresponding author.

E-mail address: wenfengyi@cup.edu.cn (W. Yi).



Fig. 1. Illustration of behavioral cascades in an emergency scenario from the film “Train to Busan”. (a) Initial stage: Upon noticing a zombie threat in the adjacent carriage, a train attendant immediately alerts passengers in the current carriage and initiates an escape behavior. (b) Intermediate stage: As the attendant quickly moves through the aisle, nearby passengers begin to respond and follow his behavior. (c) Later stage: The propagation of escape behavior triggers a rapid cascade effect among passengers, resulting in large-scale collective evasion throughout the carriage.

limitation to capture the emergent nature and evolving dynamics of behavioral change in collective human motion, which enables more accurate and responsive simulations of representative patterns during real-world evacuation.

In biological and social systems, the cascade effect of behavioral change has been widely observed and studied. For mobile animal groups, such as flocking birds and schooling fish, individual responses to information from nearby neighbors can occur over short timescales [29], resulting in rapid waves of behavioral contagion [15,30]. Previous studies have proposed behavioral contagion models to predict behavioral cascades and explore the effects of group structures, feedback mechanisms, density levels, and movement parameters on their emergence [31–34]. However, these models typically either assume static interaction networks that neglect individual mobility, or incorporate dynamic networks with simplistic motion rules, lacking a comprehensive integration of contagion dynamics and movement responses. For human societies, behavioral cascades are widespread, evident in real-world emergencies and frequently portrayed in films and media (e.g., the propagation of escape behavior in “Train to Busan”, see Fig. 1). To better reproduce such collective dynamics, many existing studies have combined crowd motion models with emotional contagion (i.e., individuals internalize and mimic the emotional states of others), whose mechanisms can be basically divided into three categories: group statistic [35,36], epidemiological [37–40], dyadic relations [41–43]. However, these models are computationally intensive and cumbersome due to their reliance on complex state variables, cognitive appraisal processes, and intricate transition rules, and are hard to validate in large-scale crowd simulations as emotional states are typically latent and indirectly inferred [13]. In contrast, behavioral contagion emphasizes the direct imitation of observable actions without requiring interpretation of emotional states. This offers a more tractable and mechanistic approach, with fewer assumptions, to model urgent collective responses, such as emergency evacuation, where escape behaviors can spread rapidly through simple observation of neighbors. Therefore, this study considers behavioral contagion as a core driver to construct a modeling framework of emergent crowd dynamics during evacuation.

In this paper, we develop a behavioral contagion-based social force model (BC-SFM) for the coupling between contagion mechanisms and movement behaviors. This model defines interaction radius and response threshold as two core parameters to characterize the perception and reaction of individuals to surrounding escape behaviors, which allows a mechanistic representation of bottom-up contagion processes in human crowds. On this basis, a series of numerical simulations are designed to systematically investigate the impact of behavioral contagion on crowd evacuation. First, the superiority of BC-SFM in describing behavioral contagion dynamics is demonstrated by comparing it with SFM in terms of response speed, evacuation efficiency, and congestion level. Second, we explore how the intensity and heterogeneity of interaction radius and response threshold influence behavioral contagion at different crowd densities, respectively. Last, the effects of

different contagion mechanisms (represented by specific combinations of perceptual capacity and individual responsiveness) on evacuation dynamics are further analyzed. The corresponding results are expected to advance our understanding of contagion mechanisms in human crowds and support the development of more realistic and predictive evacuation models.

The rest of this paper is organized as follows. Section 2 describes the mathematical form of the proposed BC-SFM. Section 3 presents numerical simulations to analyze the dynamics of behavioral contagion in crowd evacuation. Finally, main conclusions and future prospects are summarized in Section 4.

2. Model

In this section, we propose the BC-SFM to couple behavioral contagion with movement dynamics. The former describes how behavioral changes propagate through groups via local interactions, while the latter models how pedestrians adjust their motion in response to both internal states and external forces. The coupling mechanism is a state-dependent motion intent, whereby the contagion state directly modulates the input of the movement model.

2.1. Behavioral contagion process

In time-pressured, information-limited emergencies, human behavior can become highly reactive and instinctive, relying heavily on the actions of nearby individuals, which resembles the collective escape responses observed in animal groups [15]. From this, we construct an interaction network by which the behavioral change propagates across groups, where nodes represent pedestrians in human crowds, and link weights are derived based on the behavior of first responders after an initial and spontaneous startle. Empirical evidence has shown that the two most predictive features of behavioral response are the logarithm of the metric distance between individuals and the ranked angular area of the initially startled individual in the visual field of the responding individual [15,31]. For simplicity, we only consider the logarithmic metric distance since the relative importance of the ranked angular area is much weaker. The link weight w_{ij} is therefore computed as the probability of a behavioral response by pedestrian i if pedestrian j has started, as given by:

$$w_{ij} = \frac{1}{1 + \exp[-\beta_1 - \beta_2 \log(d_{ij})]} \quad (1)$$

where intercept β_1 and LMD coefficient β_2 are determined by performing a logistic regression of experimental observations of first responders, and $d_{ij} = \|x_i - x_j\|$ is the Euclidean distance between the positions of pedestrians i and j .

Each pedestrian represented by a node in an interaction network with link weights w_{ij} exists in one of two possible states: susceptible and infected. According to a continuous-time variant [34] of the Dodds

& Watts model [44], the behavioral contagion process is described as follows: A susceptible pedestrian i , moving with a desired speed $v_i^0(t) = v_i^{\text{sus}}$ in a desired direction $\mathbf{e}_i^0(t) = \mathbf{e}_i^{\text{ori}}$ toward the original destination, receives stochastic activation signals of fixed size s_a from an infected neighbor j at a rate $\rho_{ij} = \rho_{\max} w_{ij}$, where ρ_{\max} is the maximum rate of sending activation signals for $w_{ij} = 1$. Note that neighbors are determined within a local interaction range of radius R_i , since it has shown that the interaction neighborhood in human crowds is not topological, and can be approximated by a metric neighborhood [45]. The stochastic time series $s_{ij}(t)$ of activation signal received by pedestrian i from an infected neighbor j is expressed as follows:

$$s_{ij}(t) = \begin{cases} s_a, & p_a \\ 0, & 1 - p_a \end{cases} \quad (2)$$

where $p_a = \rho_{ij} \Delta t$ is the probability of receiving an activation signal per numerical time step Δt . The pedestrian integrates the stochastic time series of activation signal in the form of exponential decay to update its current cumulative signal $S_i(t)$:

$$\frac{dS_i(t)}{dt} = -\delta S_i(t - \Delta t) + \frac{1}{\Delta t} \sum_j s_{ij}(t) \quad (3)$$

where δ represents a discount factor. Eq. (3) can be rewritten by applying a standard Euler discretization:

$$S_i(t) = (1 - \delta \Delta t) S_i(t - \Delta t) + \sum_j s_{ij}(t) \quad (4)$$

Here, each pedestrian has an internal response threshold θ_i reflecting the probability of response to neighboring alarms, which implicitly represents the degree of hesitation or uncertainty in decision-making. If the cumulative signal exceeds this threshold, pedestrian i transitions to the infected state and escapes with a desired speed $v_i^0(t) = v_i^{\text{inf}}$, aligning its desired direction $\mathbf{e}_i^0(t) = \langle \mathbf{e}_j^0(t) \rangle_j$ with the normalized average direction of infected neighbors j . Once all pedestrians become infected, each will revert to the susceptible state and start moving with a desired speed $v_i^0(t) = v_i^{\text{sus}}$ in a desired direction $\mathbf{e}_i^0(t) = \mathbf{e}_i^{\text{new}}$ toward the new destination. To clarify the above behavioral contagion process, a schematic diagram is illustrated accordingly in Fig. 2.

2.2. Pedestrian movement dynamics

The SFM [19] is used to simulate the movement dynamics of pedestrians. The position $\mathbf{x}_i(t)$ of pedestrian i is updated by:

$$\frac{d\mathbf{x}_i(t)}{dt} = \mathbf{v}_i(t) \quad (5)$$

where the change of velocity $\mathbf{v}_i(t)$ is updated by the acceleration equation:

$$m_i \frac{d\mathbf{v}_i(t)}{dt} = \mathbf{f}_{id} + \sum_{j(\neq i)} \mathbf{f}_{ij} + \sum_W \mathbf{f}_{iW} \quad (6)$$

The first term \mathbf{f}_{id} is a self-driven force that propels pedestrians toward the destination:

$$\mathbf{f}_{id} = m_i \frac{v_i^0(t) \mathbf{e}_i^0(t) - \mathbf{v}_i(t)}{\tau_i} \quad (7)$$

Here, pedestrian i of mass m_i adapts the actual velocity $\mathbf{v}_i(t)$ within a characteristic time τ_i to move with a desired speed $v_i^0(t)$ in a desired direction $\mathbf{e}_i^0(t)$, which are determined by the contagion state (i.e., susceptible or infected) of pedestrian i .

The second term \mathbf{f}_{ij} is an interaction force with other pedestrians j :

$$\mathbf{f}_{ij} = A_i \exp \left[(r_{ij} - d_{ij}) / B_i \right] \mathbf{n}_{ij} + kg (r_{ij} - d_{ij}) \mathbf{n}_{ij} + \kappa g (r_{ij} - d_{ij}) \Delta u_{ji}^t \mathbf{t}_{ij} \quad (8)$$

where A_i and B_i are constants, r_{ij} denotes the sum of their radii r_i and r_j , and \mathbf{n}_{ij} is the normalized vector pointing from pedestrian j to i . k

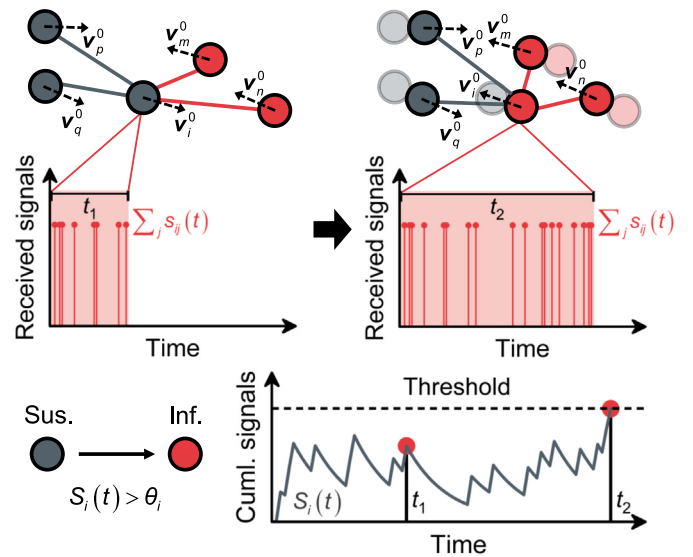


Fig. 2. Schematic diagram of the behavioral contagion process. The focal susceptible pedestrian (gray) continuously receives activation signals from neighboring infected pedestrians (red), which are integrated over time to produce a cumulative quantity $S_i(t)$. At an earlier time t_1 , the cumulative signal remains below the response threshold. Thus, the focal pedestrian stays in the susceptible state and continues moving with its current desired velocity. As pedestrians move and their relative positions shift, the received signal strengths change dynamically. Eventually, the cumulative signal exceeds the response threshold at time t_2 , triggering a transition to the infected state. The focal pedestrian then updates its desired velocity and adjusts movement accordingly. Note that the vector v_i^0 of the desired velocity is composed of a desired speed v_i^0 along a desired direction \mathbf{e}_i^0 .

and κ are body elasticity coefficient and sliding friction coefficient, \mathbf{t}_{ij} is the tangential direction, and Δu_{ji}^t is the tangential velocity difference. Note that $g(x)$ is zero if pedestrians i and j do not touch each other, otherwise it equals to the argument x .

The last term \mathbf{f}_{iW} is a similar interaction force with wall W :

$$\mathbf{f}_{iW} = A_i \exp \left[(r_i - d_{iW}) / B_i \right] \mathbf{n}_{iW} + kg (r_i - d_{iW}) \mathbf{n}_{iW} - \kappa g (r_i - d_{iW}) (\mathbf{v}_i \cdot \mathbf{t}_{iW}) \mathbf{t}_{iW} \quad (9)$$

where d_{iW} is the Euclidean distance to wall W , \mathbf{n}_{iW} is the normalized vector perpendicular to it, and \mathbf{t}_{iW} the direction tangential to it.

3. Numerical simulations

3.1. Experiment setup

To simulate the behavioral contagion process of evacuated pedestrians, as shown in Fig. 3, we design a T-shaped corridor as the simulation scenario. The horizontal branch (40 m \times 6 m) is a connecting passage leading to two available exits of 2 m width, Exit A (green strip) and Exit B (orange strip), located on the left and right sides. The vertical branch (10 m \times 14 m) serves as the initial area (gray rectangle), where pedestrians are uniformly distributed at the start of the simulation. Pedestrians should traverse a longer route (left passage of 20 m length) if they choose Exit A, but only need to cover a shorter route (right passage of 10 m length) to Exit B. Here, a simulation constraint is imposed that Exit B is inaccessible (e.g., blocked). To construct limited visibility conditions such as in a smoky environment, we assume that pedestrians are unaware of this situation until entering the awareness area (light orange rectangle) within 2 m of Exit B [19], after which they will change their decisions and escape toward Exit A instead.

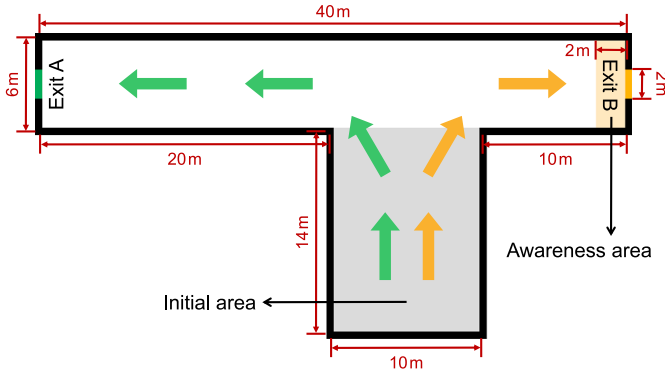


Fig. 3. Schematic diagram of the T-shaped corridor. The green and orange strips denote Exit A and Exit B, and black bars represent walls. The gray rectangle indicates the initial area where pedestrians are uniformly generated, and the light orange rectangle marks the awareness area in front of Exit B. The green and orange arrows indicate possible escape flows toward Exit A and Exit B, respectively.

The parameter settings of this model are described below. For behavioral contagion, due to the lack of available human data, parameter values are empirically informed by animal experiments [31,34] and provide plausible approximations for contagion dynamics. The intercept $\beta_1 = -0.271$ and LMD coefficient $\beta_2 = -2.737$ in the logistic regression model are fitted from experimental data. The maximal rate $\rho_{\max} = 10^2 \text{ s}^{-1}$ allows the fastest response time to be the order of 0.01 s (for $w_{ij} = 1$), and therefore the numerical time step is equal to $\Delta t = 1/\rho_{\max} = 0.01$ s. Without loss of generality, $s_a\rho_{\max} = 1$, the size of activation signal is set to $s_a = 10^{-2}$ if the maximal rate $\rho_{\max} = 10^2 \text{ s}^{-1}$. With the discount factor $\delta = 0.1$ we have a reasonable decay rate for the cumulative signal. For movement dynamics, parameter values are taken from the well-established SFM [19], which have been extensively applied and validated in numerous studies. The mass and radius of pedestrians are set to $m_i = 80 \text{ kg}$ and $r_i = 0.25 \text{ m}$, and the characteristic time $\tau_i = 0.5$ s is a frequently used estimation. The two constants $A_i = 2 \cdot 10^3 \text{ N}$ and $B_i = 0.08 \text{ m}$ can well describe the intensity and range of repulsive interaction between pedestrians. The body elasticity coefficient $k = 1.2 \cdot 10^5 \text{ kgs}^{-2}$ and sliding friction coefficient $\kappa = 2.4 \cdot 10^5 \text{ kgm}^{-1}\text{s}^{-1}$ govern the obstructive effects resulting from physical interactions. The values of remaining parameters not mentioned here will be given later depending on specific simulation conditions.

3.2. Performance comparison between SFM and BC-SFM

The first part of our simulations aims to validate the performance superiority of BC-SFM by comparing it with SFM (the most classical crowd motion model). Here, we set up a representative evacuation situation in which a total of $N = 100$ pedestrians, randomly generated in the initial area, simultaneously perceive a danger signal (e.g., explosion, earthquake) and move toward the closer Exit B. After a while, pedestrians who realize that Exit B is inaccessible (i.e., entering the awareness area or being infected by active neighbors) will immediately reverse direction and escape toward the more distant Exit A. Given that pedestrians exhibit heterogeneity in both psychological and physiological aspects in reality [22,23], it is assumed that the values of their desired speeds are randomly sampled from a uniform distribution $U(2 \text{ ms}^{-1}, 4 \text{ ms}^{-1})$ and remain consistent in both susceptible and infected states ($v_i^{\text{sus}} = v_i^{\text{inf}}$). For the two key parameters of BC-SFM, we set interaction radius $R_i = 1 \text{ m}$ and response threshold $\theta_i = 0.4$ as an example to reasonably simulate the behavioral contagion process. It is worth noting that all simulations for quantitative analysis are repeated 50 times to minimize the influence of stochastic fluctuations,

with identical parameters in SFM and BC-SFM being assigned the same values for each corresponding run.

From a qualitative perspective, Fig. 4(a)–(b) display the spatio-temporal snapshots of the behavioral change process during evacuation simulated by SFM and BC-SFM. In the initial stage, both SFM (before $t = 6$ s) and BC-SFM (before $t = 4$ s) present similar evacuation dynamics. All pedestrians spontaneously start to move upon perceiving the danger, while a few individuals at the front of the crowd find that Exit B is inaccessible after entering the awareness area, thus promptly redirecting their movement direction toward the farther Exit A. However, significant differences emerge during the subsequent stages of evacuation. The phenomenon simulated by SFM (after $t = 12$ s) indicates that behavioral change is solely triggered by individuals themselves upon entering the awareness area, without any propagation effects from neighboring individuals. Hence, the spatially localized awareness leads to severe delay and congestion near Exit B. In contrast, BC-SFM (after $t = 8$ s) successfully characterizes the spread of behavioral change through local interactions from active neighbors, without the necessity for direct perception. This results in a more rapid and collective redirection toward Exit A, thereby alleviating delay and congestion. Overall, the behavioral change process during evacuation simulated by BC-SFM appears more coordinated and realistic than that of SFM, which resembles a behavior where individuals completely distrust the actions of active neighbors and rely solely on their own direct awareness to make decisions.

To quantitatively demonstrate the performance superiority of our model in reflecting behavioral change during evacuation, we provide a comprehensive comparison between SFM and BC-SFM across several key indicators in Fig. 5. Fig. 5(a) illustrates the distributions of individual onset t_i^{ons} (i.e., the activation time at which each pedestrian changes behavior) and collective duration t^{dur} (i.e., the total time span from the first to the last behavioral change). BC-SFM exhibits faster and more synchronized individual responses, as evidenced by a more concentrated distribution of the onset time with lower variability. Meanwhile, the collective duration is significantly shorter, implying that the contagion mechanism embedded in BC-SFM effectively reproduces the spread of behavioral cascades. However, the broader distributions of individual onset and collective duration in SFM indicate that such a coordinated shift in group decision cannot be clearly reflected, as behavioral change depends purely on direct personal perception. The self-triggered (non-propagative) response indirectly leads to substantial delays in the overall evacuation time in Fig. 5(b) and extremely high congestion levels [46] near Exit B, as shown in Fig. 5(c), while the blockage near Exit A is mild due to the staggered arrival of redirected pedestrians. Turning to BC-SFM, the rapid transmission of directional information relieves the localized flow stagnation in which aware pedestrians trying to redirect are obstructed by unaware ones still heading toward Exit B. This largely improves the evacuation efficiency in Fig. 5(b), but slightly aggravates the congestion level near Exit A in Fig. 5(c) due to the closely clustered arrival of redirected pedestrians. In summary, these results highlight the unique advantage of BC-SFM over traditional models in characterizing the dynamical process of behavioral contagion during evacuation.

3.3. Effects of interaction radius and response threshold on behavioral contagion

In this section, we are interested in how the two key parameters of BC-SFM affect the behavioral adaptation process. We adjust the three levels of crowd density by setting the number of pedestrians to $N = 50$ (low density), $N = 100$ (medium density), and $N = 150$ (high density). The interaction radius R_i defines the maximum distance within which pedestrians can perceive the behavioral states of surrounding individuals, that is, those only closer to the focal pedestrian ($d_{ij} < R_i$) are regarded as its neighbors with social influence [45]. The response threshold θ_i quantifies the minimum cumulative signals required for

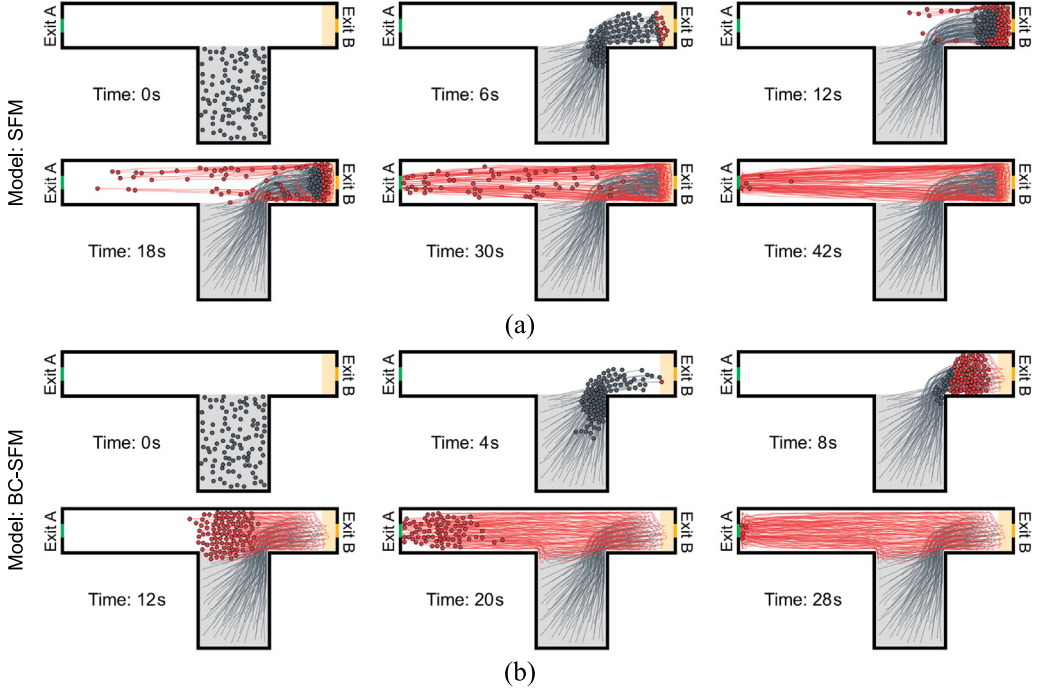


Fig. 4. Spatio-temporal snapshots of the behavioral change process during evacuation. (a) Simulated by SFM. (b) Simulated by BC-SFM. Pedestrians are represented by circles and their trajectories by curves, with gray and red colors indicating states before and after behavioral changes, respectively.

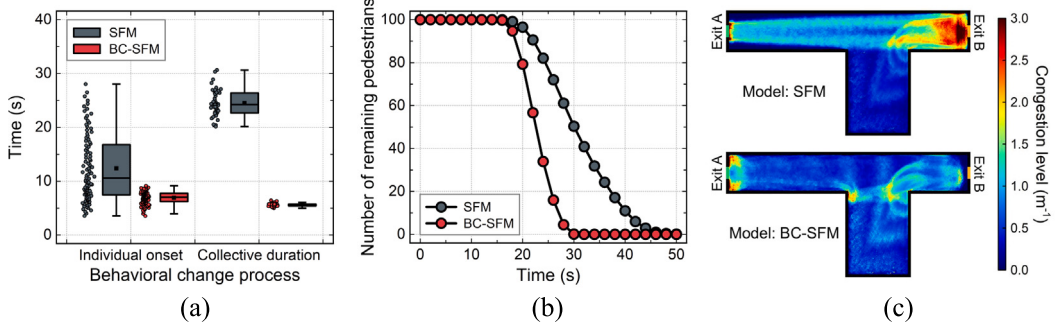


Fig. 5. Quantitative comparison of the simulation performance of SFM and BC-SFM. (a) Box plot of individual onset and collective duration in the behavioral change process. (b) Number of remaining pedestrians as a function of time. (c) Spatial characterization of congestion level in the scenario.

a pedestrian to change behavior ($S_i > \theta_i$), which means the level of activation stimulus the focal pedestrian tolerates before itself being infected. To better understand the direct effects of these two parameters, three evaluation indicators are introduced here: First, the infection ratio n_{inf}/N represents the number of infected pedestrians (i.e., induced by behavioral contagion rather than entry into the awareness area) divided by the total number of pedestrians, which measures the dominant role of contagion in behavioral transition. Second, the average activation onset $\langle t_i^{\text{ons}} \rangle_i$ is defined as the average time at which pedestrians first change their behaviors, thereby reflecting the propagation speed of behavioral change within the crowd. Third, the average body compression exerting on each pedestrian per time step is $\langle C_i(t) \rangle_{i,t}$, where $C_i(t) = \sum_j \|f_{ij}\|$ is the sum of the contact forces [47] with other individuals applied to pedestrian i at time t , and this indicator assesses the intensity of crowd pushing during the process of behavioral cascades.

The effects of the intensity levels of interaction radius and response threshold on behavioral contagion at different crowd densities are investigated in Fig. 6. The interaction radius R_i is traversed from 0.5 m to 2.0 m at intervals of 0.15 m, and the response threshold θ_i is sampled from 0 to 2.0 at intervals of 0.2. Fig. 6(a)–(c) demonstrate that the infection ratio consistently grows with increasing R_i and

decreasing θ_i . A larger R_i allows pedestrians to access more activated neighbors and a lower θ_i reduces the cumulative stimulus required for behavioral change, these conditions together facilitate faster and more extensive contagion across the crowd. Notably, the infection ratio gradually rises under the same parameter conditions as crowd density increases from low to high. This is because a higher density enhances both the probability of close contacts and the effective number of neighbors within an interaction range. The average activation onset in Fig. 6(d)–(f) accelerates as R_i increases and θ_i decreases, denoting that pedestrians will respond more quickly if they are affected by more neighbors and require less stimulus to be infected. Interestingly, the increase in crowd density amplifies the polarization of the average activation onset. That is, stronger interpersonal connectivity promotes propagation at larger R_i and lower θ_i by producing faster signal accumulation, but suppresses propagation at smaller R_i and higher θ_i by reinforcing locally enclosed structures. In Fig. 6(g)–(i), the average body compression peaks near the diagonal region due to behavioral synchronization from different mechanisms. If both R_i and θ_i are lower (left-bottom), individuals are highly sensitive and rapidly synchronize within their local vicinity, and such rapid local activation leads to sudden bursts of movement and intense localized compression even if

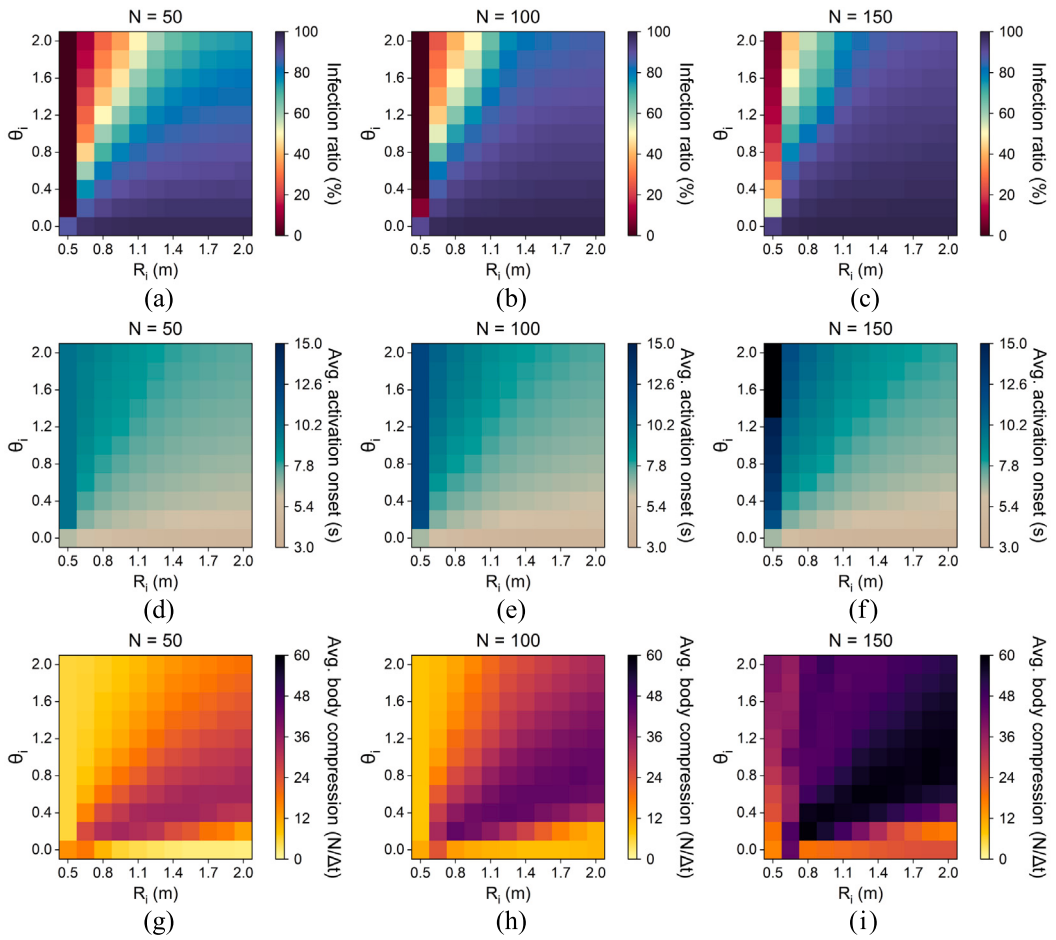


Fig. 6. Effects of the intensity levels of interaction radius and response threshold on behavioral contagion at different crowd densities. (a)–(c) Infection ratio. (d)–(f) Average activation onset. (g)–(i) Average body compression.

their perception ranges are limited. If both R_i and θ_i are larger (right-upper), individuals react more slowly, but once activated, the wide perception range enables broad coordination, which results in delayed yet large-scale synchronization and strong global compression. For non-diagonal regions, larger R_i and lower θ_i (right-bottom) facilitate rapid and large-scale synchronization, behavioral contagion occurs almost immediately once the stimulus appears, this early and global shift in group behavior can minimize physical conflicts. The condition of lower R_i and higher θ_i (left-upper) makes behavioral contagion hard to initiate and spread sparsely, therefore, the prolonged adaptation process dilutes instantaneous conflicts even if congestion remains. It can be concluded that the interaction radius and response threshold jointly modulate both the temporal efficiency and spatial coordination of behavioral contagion.

Due to the diverse characteristics of pedestrians in human crowds, the effects of the heterogeneity levels of interaction radius and response threshold on behavioral contagion are further explored in Fig. 7. These two parameters are assumed to follow uniform distributions $R_i \sim U((1 - \lambda_R)\bar{R}_i, (1 + \lambda_R)\bar{R}_i)$ and $\theta_i \sim U((1 - \lambda_\theta)\bar{\theta}_i, (1 + \lambda_\theta)\bar{\theta}_i)$, where $\bar{R}_i = 1.25$ m and $\bar{\theta}_i = 1.0$ are the average values, λ_R and λ_θ are the heterogeneity levels, ranging from 0 to 1 in increments of 0.1. The decreasing λ_R and increasing λ_θ lead to a steady growth of the infection ratio in Fig. 7(a)–(c) and a tendency for activation onset to occur earlier in Fig. 7(d)–(f). A lower λ_R implies that most individuals have similar perceptual ranges, and this perceptual uniformity can ensure that activation signals are transmitted more continuously among individuals and avoid the case where the contagion chain is interrupted by isolated “perceptual blind spots”. A higher λ_θ means there are

more “sensitive individuals”, who will be activated quickly and act as amplifiers to trigger responses in their neighbors, thus forming behavioral cascades, and even high-threshold individuals are more likely to be activated by the continued stimulus. In addition, the growing density level intensifies interpersonal interactions and enhances the likelihood of stimulus accumulation across the group, resulting in a higher infection ratio under the same heterogeneity settings. However, it also makes the delay effect more pronounced (i.e., heterogeneity causes individuals with high thresholds or limited perception to be activated later), slightly prolonging the average activation onset. Fig. 7(g)–(i) illustrate how average body compression varies with λ_R and λ_θ across different crowd densities. At low and moderate densities in Fig. 7(g)–(h), body compression appears sporadic and weakly structured, indicating that individual heterogeneity has limited influence under relatively sparse conditions. At high density in Fig. 7(i), body compression is significantly higher in a certain zone where both λ_R and λ_θ are lower (i.e., both R_i and θ_i are moderate, as shown in the center of the diagonal region in Fig. 6). In this case, individuals have similar perceptual ranges and responsiveness to activation stimuli, they respond in a coordinated yet not overly scattered manner, and the mid-scale synchronization may cause bursts of movement and exacerbate body compression. Outside the left-bottom region, most individuals act in a more asynchronous way as either or both heterogeneities increase, this disperses the spatio-temporal concentration of behavioral transitions, thereby reducing simultaneous movements and mitigating crowd pressure. In summary, these results highlight the key role of individual heterogeneity in affecting behavioral contagion and collective patterns under different density conditions.

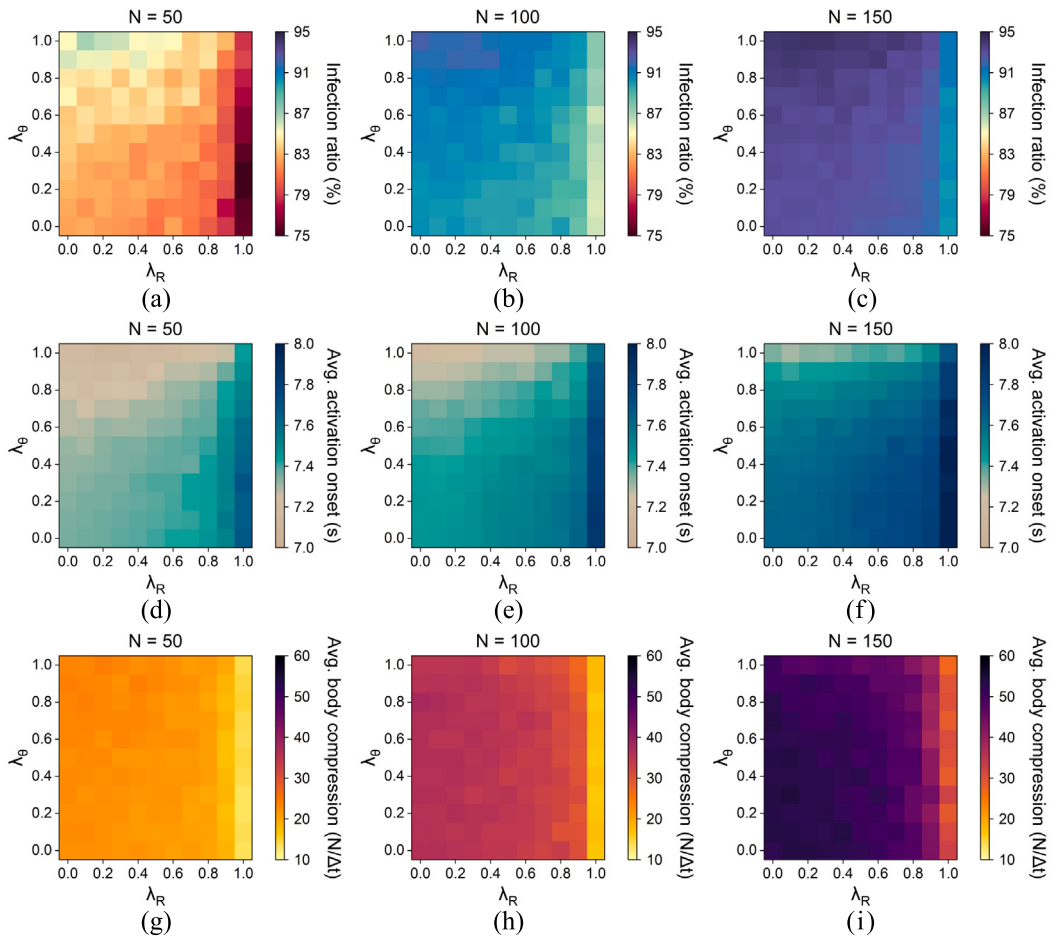


Fig. 7. Effects of the heterogeneity levels of interaction radius and response threshold on behavioral contagion at different crowd densities. (a)–(c) Infection ratio. (d)–(f) Average activation onset. (g)–(i) Average body compression.

3.4. Analysis of evacuation dynamics under different contagion mechanisms

This section is concerned with systematically studying the joint effects of perceptual capacity and individual responsiveness on evacuation dynamics, two representative intervals are selected for each parameter: short-range [0.5 m, 0.8 m] and long-range [1.7 m, 2.0 m] for interaction radius R_i , and low-threshold [0, 0.4] and high-threshold [1.6, 2.0] for response threshold θ_i . Accordingly, we construct a simulation framework based on four typical pedestrian types, which are derived from different combinations of interaction radius and response threshold. Type 1 (short-range $R_i \in [0.5 \text{ m}, 0.8 \text{ m}]$ and low-threshold $\theta_i \in [0, 0.4]$): individuals are characterized by limited perceptual range but high responsiveness, making them highly prone to mimic nearby behaviors and thus capable of triggering rapid yet localized synchronization. Type 2 (short-range $R_i \in [0.5 \text{ m}, 0.8 \text{ m}]$ and high-threshold $\theta_i \in [1.6, 2.0]$): individuals exhibit both limited perception and high resistance to activation, often resulting in delayed or suppressed behavioral contagion across the group. Type 3 (long-range $R_i \in [1.7 \text{ m}, 2.0 \text{ m}]$ and low-threshold $\theta_i \in [0, 0.4]$): individuals, with extensive perception and low activation thresholds, respond simultaneously and rapidly to activation cues, thereby promoting large-scale and accelerated behavioral contagion. Type 4 (long-range $R_i \in [1.7 \text{ m}, 2.0 \text{ m}]$ and high-threshold $\theta_i \in [1.6, 2.0]$): individuals combine high perceptual capability with low behavioral sensitivity, yielding slightly slower collective responses, but once activated, their wide perception promotes broad and coordinated synchronization. This framework provides a controlled basis for comparatively analyzing the evacuation dynamics under varying conditions of perceptual capacity and individual responsiveness.

Fig. 8 displays the spatio-temporal snapshots of the evacuation process simulated by BC-SFM under four typical pedestrian types. In the early stage (before $t = 4 \text{ s}$), all types start with the same initial distribution ($N = 100$), and the individual closest to Exit B acts as an initiator of behavioral change upon perceiving danger. However, their subsequent collective dynamics diverge markedly due to differences in perceptual and responsive traits. Type 2 exhibits the slowest evacuation process in **Fig. 8(b)**, the lack of perceptual connectivity and high activation thresholds inhibits the spread of behavioral change, resulting in prolonged stagnation and inefficient use of the alternative exit. The crowd remains clustered near the blocked Exit B for an extended period, with little sign of coordination or adaptation. In stark contrast, Type 3 achieves the fastest evacuation efficiency in **Fig. 8(c)**. Once a few individuals detect the inaccessibility of Exit B, behavioral change rapidly propagates across the crowd, and all pedestrians are redirected toward Exit A in a highly synchronized manner. The swift and cohesive transition reveals the emerging dynamics under broad perceptual range and low resistance to activation. Between these two extremes, both Types 1 and 4 in **Fig. 8(a)** and **8(d)** present moderate evacuation efficiencies, but their spatial patterns have certain differences. In the first half of the contagion process ($t = 8 \text{ s}$), the behavioral change in Type 1 spreads more rapidly than that in Type 4, because the high responsiveness allows quick imitation of nearby activated neighbors. Nonetheless, several inactive individuals are visibly trapped within clusters of already-activated ones, implying that the contagion remains highly localized due to the limited perceptual range. Although the case in Type 4 is slower to take effect because of high response thresholds, individuals with a wide perception scope enable faster and more coherent collective responses. Thus, the contagion process accelerates and

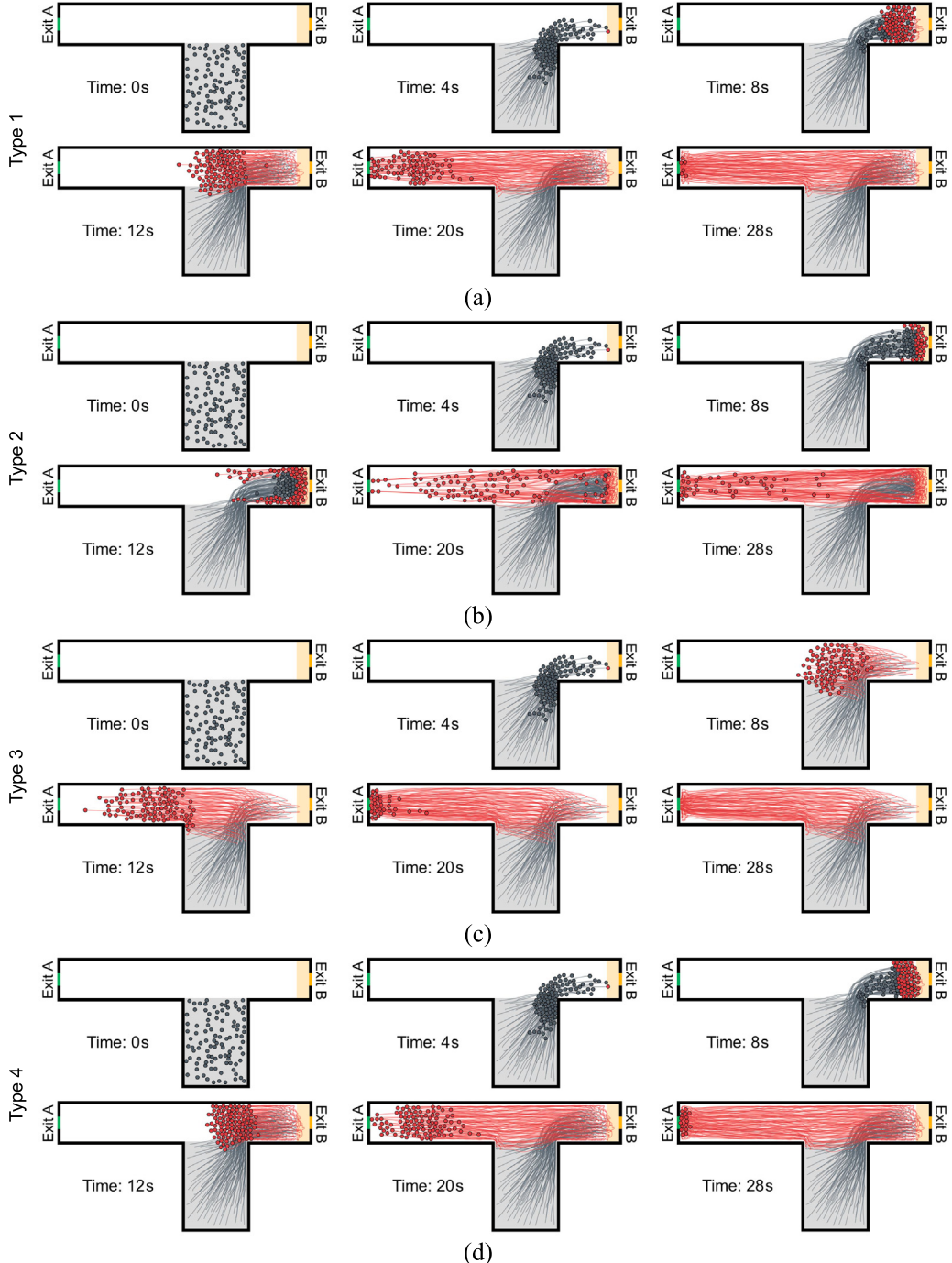


Fig. 8. Spatio-temporal snapshots of the evacuation process simulated by BC-SFM. (a) Type 1 (short-range and low-threshold). (b) Type 2 (short-range and high-threshold). (c) Type 3 (long-range and low-threshold). (d) Type 4 (long-range and high-threshold). Pedestrians are represented by circles and their trajectories by curves, with gray and red colors indicating states before and after behavioral changes.

catches up with that of Type 1, ultimately achieving a more coordinated redirection in the latter part of the contagion process ($t = 12$ s). To sum up, Type 1 enables rapid local reactions but fragmented coordination, Type 2 presents the weakest contagion and longest delay, Type 3 ensures the fastest and most synchronized evacuation, and Type 4 shows more uniform adaptation with slower initial responses.

To further quantitatively compare the evacuation dynamics across four typical pedestrian types, Fig. 9 presents the temporal evolutions of infected pedestrians, remaining pedestrians, and congestion level at different crowd densities. Fig. 9(a)–(c) plot the number of infected pedestrians over time, serving as a proxy of contagion speed. Type 3

shows the steepest and earliest rising curves, reaching global infection rapidly, whereas Type 2 displays the flattest and most delayed growth, with curves taking the longest to plateau. Type 1 exhibits a relatively faster initial increase, but gradually levels off before reaching full saturation. Type 4 has a slower initial rise but the curve grows steadily over time, eventually approaching or surpassing Type 1. Notably, as the crowd density increases, the differences among the four types become more significant. This divergence arises since higher density intensifies spatial interference and movement constraints, which hinders information transmission for types relying on limited perception or high activation thresholds, while amplifying the advantage of those with

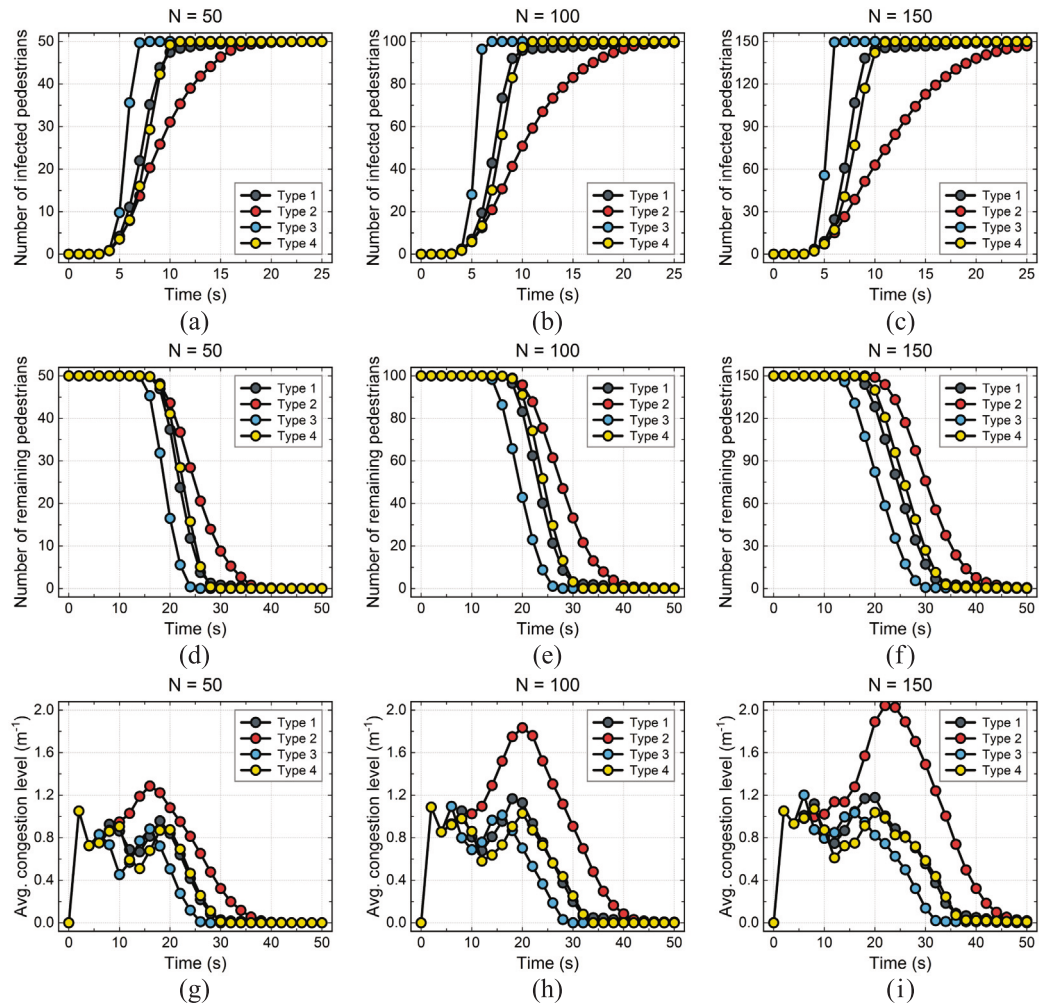


Fig. 9. Quantitative analysis of the evacuation process for four typical pedestrian types at different crowd densities. (a) Number of infected pedestrians as a function of time. (b) Number of remaining pedestrians as a function of time. (c) Average congestion level as a function of time.

broader awareness and lower resistance to activation. The trends of the number of remaining pedestrians in Fig. 9(d)–(f) are quite consistent with spatio-temporal patterns in Fig. 8. The observed variation in evacuation efficiency primarily stems from the contagion dynamics in Fig. 9(a)–(c), where faster and more synchronized infection facilitates earlier behavioral transitions and more coordinated redirection, thereby accelerating the overall evacuation. In addition, the temporal evolution of average congestion level is depicted in Fig. 9(g)–(i). Types 1, 3, and 4 exhibit two-peak structures: an initial peak caused by early accumulation near Exit B, followed by a second peak as redirected pedestrians converge at Exit A. Here, Type 3 shows the earliest and lowest second peak, highlighting that fast and synchronized contagion enables pedestrians to shift toward Exit A with minimal delay and congestion. Type 4 also achieves a low second peak, though it appears later, reflecting a slower initial response but rapid emergence of global synchronization once contagion spreads, which promotes coordinated flow without abrupt surges. Type 1 presents a higher and delayed second peak, as fast but local contagion limits group-level coordination, leading to persistent arrivals at Exit A with temporary crowding. A notable exception is Type 2, which only displays a single and the highest peak among all types. This is because pedestrians mostly gather near Exit B for a long time and sluggishly reroute toward Exit A, the delayed and uncoordinated shift triggers extreme congestion. The peak congestion of Type 2 escalates dramatically as density increases, whereas the peaks of Types 1, 3, and 4 rise only slightly, implying their greater adaptability to crowded conditions. In essence, the evacuation

dynamics across the four pedestrian types underscore the key role of contagion mechanisms in shaping collective human behavior.

4. Conclusions

In this work, we propose a systematic modeling framework to simulate the dynamical process of behavioral contagion in human crowds during evacuation. By incorporating contagion dynamics into the SFM, we explore how microscopic propagation mechanisms, mediated by parameters such as interaction radius and response threshold, affect macroscopic decision-making and collective motion in crowd evacuation. Numerical simulations reveal several crucial findings: (1) Compared with the SFM, the proposed BC-SFM reproduces the spatio-temporal dynamics of behavioral contagion more realistically, which enables faster redirection and reduces congestion near the blocked exit. (2) The intensities of interaction radius and response threshold regulate the speed and coordination of behavioral contagion, and their heterogeneity modulates contagion continuity, activation timing, and synchronization level in collective evasion maneuvers. (3) Different combinations of perceptual capacity and individual responsiveness lead to distinct contagion mechanisms, which in turn influence the escape efficiency and congestion level of evacuation dynamics.

This work provides valuable inspiration for understanding and managing behavioral cascades in human crowds, and offers theoretical guidance for the design of evacuation strategies and swarm robotics. On the one hand, this model can support the development of real-time

crowd management systems in scenarios such as sports stadiums or festival events, where spontaneous crowd reactions are highly sensitive to local disruptions. By adjusting key contagion parameters, authorities can explore scenario-based interventions to optimize spatial layouts or route planning [48,49], and can also inform the placement of visual signage, auditory alerts, or localized guidance agents [50,51] to influence early responders and steer behavioral contagion toward safer evacuation patterns. On the other hand, beyond human evacuation, the modeling principles are also transferable to swarm robotics, such as drone fleets [52] or autonomous delivery systems [53]. The local communication and imitation mechanisms can be designed to support coordinated rerouting, obstacle avoidance, and emergent decision-making [54]. In such systems, tuning contagion-inspired interaction rules is expected to enhance the adaptability and robustness of swarm robotics in dynamic and uncertain environments.

Despite its contributions, this work has several limitations that point toward future research directions. First, contagion parameters in this model, while empirically inspired by animal experiments, have not yet been calibrated with human data. This potentially limits its ability to predict real-world contagion dynamics in human crowds, and future work may address this limitation through controlled human experiments or virtual reality technology for more accurate parameter estimation and enhanced model reliability. Second, although our model characterizes basic contagion mechanisms, it does not yet account for higher-level social dynamics [25] such as role differentiation, hierarchy formation, and antagonistic interactions, all of which play critical roles in emergency evacuation situations. Future studies should aim to enrich contagion-movement coupling models by incorporating multimodal perception, adaptive decision-making rules, and empirically based psychological factors. Furthermore, systematic validation using controlled experiments or real-world datasets will be essential to improve model realism and extend its applicability to practical crowd management.

CRediT authorship contribution statement

Wenhan Wu: Writing – original draft, Visualization, Validation, Supervision, Software, Methodology, Investigation, Formal analysis, Writing – review & editing. **Wenfeng Yi:** Writing – original draft, Validation, Resources, Project administration, Methodology, Funding acquisition, Conceptualization, Writing – review & editing.

Declaration of competing interest

The authors declare that they have no known competing financial interests or personal relationships that could have appeared to influence the work reported in this paper.

Acknowledgments

This research was supported by Science Foundation of China University of Petroleum, Beijing (No. 2462025YJRC020).

Data availability

Data will be made available on request.

References

- [1] Dong H, Zhou M, Wang Q, Yang X, Wang F-Y. State-of-the-art pedestrian and evacuation dynamics. *IEEE Trans Intell Transp Syst* 2020;21(5):1849–66. <http://dx.doi.org/10.1109/tits.2019.2915014>.
- [2] Bakhshian E, Martinez-Pastor B. Evaluating human behaviour during a disaster evacuation process: A literature review. *J Traffic Transp Eng (English Edition)* 2023;10(4):485–507. <http://dx.doi.org/10.1016/j.jtte.2023.04.002>.
- [3] Chen X, Treiber M, Kanagaraj V, Li H. Social force models for pedestrian traffic – state of the art. *Transp Rev* 2017;38(5):625–53. <http://dx.doi.org/10.1080/01441647.2017.1396265>.
- [4] Li Y, Chen M, Dou Z, Zheng X, Cheng Y, Mebarki A. A review of cellular automata models for crowd evacuation. *Phys A* 2019;526:120752. <http://dx.doi.org/10.1016/j.physa.2019.03.117>.
- [5] Senanayake GP, Kien M, Zou Y, Dirks K. Agent-based simulation for pedestrian evacuation: A systematic literature review. *Int J Disaster Risk Reduct* 2024;111:104705. <http://dx.doi.org/10.1016/j.ijdr.2024.104705>.
- [6] Li S, Zhuang J, Shen S. A three-stage evacuation decision-making and behavior model for the onset of an attack. *Transp Res Part C: Emerg Technol* 2017;79:119–35. <http://dx.doi.org/10.1016/j.trc.2017.03.008>.
- [7] Zhou Z-X, Nakanishi W, Asakura Y. Route choice in the pedestrian evacuation: Microscopic formulation based on visual information. *Phys A* 2021;562:125313. <http://dx.doi.org/10.1016/j.physa.2020.125313>.
- [8] Yi W, Wu W, Wang X, Zheng X. Modeling the mutual anticipation in human crowds with attention distractions. *IEEE Trans Intell Transp Syst* 2023;24(9):10108–17. <http://dx.doi.org/10.1109/tits.2023.3268315>.
- [9] Helbing D, Johansson A. Pedestrian, crowd and evacuation dynamics. In: Encyclopedia of complexity and systems science. Springer New York; 2009, p. 6476–95. http://dx.doi.org/10.1007/978-0-387-30440-3_382.
- [10] He Z, Shen K, Lan M, Weng W. The effects of dynamic multi-hazard risk assessment on evacuation strategies in chemical accidents. *Reliab Eng Syst Saf* 2024;246:110044. <http://dx.doi.org/10.1016/j.ress.2024.110044>.
- [11] Lu P, Li Y. Agent-based fire evacuation model using social learning theory and intelligent optimization algorithms. *Reliab Eng Syst Saf* 2025;260:111000. <http://dx.doi.org/10.1016/j.ress.2025.111000>.
- [12] Zou H, Su H, Song S, Zhu J. Understanding human behaviors in crowds by imitating the decision-making process. *Proc AAAI Conf Artif Intell* 2018;32(1). <http://dx.doi.org/10.1609/aaai.v32i1.12316>.
- [13] van Haeringen ES, Gerritsen C, Hindriks KV. Emotion contagion in agent-based simulations of crowds: a systematic review. *Auton Agents Multi-Agent Syst* 2022;37(1). <http://dx.doi.org/10.1007/s10458-022-09589-z>.
- [14] Ma Y, Lee EWM, Shi M, Yuen RKK. Spontaneous synchronization of motion in pedestrian crowds of different densities. *Nat Hum Behav* 2021;5(4):447–57. <http://dx.doi.org/10.1038/s41562-020-00997-3>.
- [15] Rosenthal SB, Twomey CR, Hartnett AT, Wu HS, Couzin ID. Revealing the hidden networks of interaction in mobile animal groups allows prediction of complex behavioral contagion. *Proc Natl Acad Sci* 2015;112(15):4690–5. <http://dx.doi.org/10.1073/pnas.1420068112>.
- [16] Gallup AC, Hale JJ, Sumpter DJT, Garnier S, Kacelnik A, Krebs JR, et al. Visual attention and the acquisition of information in human crowds. *Proc Natl Acad Sci* 2012;109(19):7245–50. <http://dx.doi.org/10.1073/pnas.1116141109>.
- [17] Múgica J, Torrents J, Cristín J, Puy A, Miguel MC, Pastor-Satorras R. Scale-free behavioral cascades and effective leadership in schooling fish. *Sci Rep* 2022;12(1). <http://dx.doi.org/10.1038/s41598-022-14337-0>.
- [18] Helbing D, Molnár P. Social force model for pedestrian dynamics. *Phys Rev E* 1995;51(5):4282–6. <http://dx.doi.org/10.1103/physreve.51.4282>.
- [19] Helbing D, Farkas I, Vicsek T. Simulating dynamical features of escape panic. *Nature* 2000;407(6803):487–90. <http://dx.doi.org/10.1038/35035023>.
- [20] Meng Q, Zhou M, Liu J, Dong H. Pedestrian evacuation with herding behavior in the view-limited condition. *IEEE Trans Comput Soc Syst* 2019;6(3):567–75. <http://dx.doi.org/10.1109/tcss.2019.2915772>.
- [21] Wu W, Yi W, Wang X, Zheng X. A vision-driven model based on cognitive heuristics for simulating subgroup behaviors during evacuation. *IEEE Trans Intell Transp Syst* 2024;25(11):16048–58. <http://dx.doi.org/10.1109/tits.2024.3421626>.
- [22] Wu W, Chen M, Li J, Liu B, Zheng X. An extended social force model via pedestrian heterogeneity affecting the self-driven force. *IEEE Trans Intell Transp Syst* 2022;23(7):7974–86. <http://dx.doi.org/10.1109/tits.2021.3074914>.
- [23] Wu W, Li J, Yi W, Zheng X. Modeling crowd evacuation via behavioral heterogeneity-based social force model. *IEEE Trans Intell Transp Syst* 2022;23(9):15476–86. <http://dx.doi.org/10.1109/tits.2022.3140823>.
- [24] Cao RF, Lee EWM, Yuen ACY, Chan QN, Xie W, Shi M, et al. Development of an evacuation model considering the impact of stress variation on evacuees under fire emergency. *Saf Sci* 2021;138:105232. <http://dx.doi.org/10.1016/j.ssci.2021.105232>.
- [25] Templeton A, Xie H, Gwynne S, Hunt A, Thompson P, Köster G. Agent-based models of social behaviour and communication in evacuations: A systematic review. *Saf Sci* 2024;176:106520. <http://dx.doi.org/10.1016/j.ssci.2024.106520>.
- [26] Guo C, Huo F, Li Y, Li C, Zhang J. An evacuation model considering pedestrian crowding and stampede under terrorist attacks. *Reliab Eng Syst Saf* 2024;249:110230. <http://dx.doi.org/10.1016/j.ress.2024.110230>.
- [27] Feng X, Jiang Y, Gai W. Rural community response to accidental toxic gas release: An individual emergency response model during self-organized evacuations. *Reliab Eng Syst Saf* 2024;248:110178. <http://dx.doi.org/10.1016/j.ress.2024.110178>.
- [28] Moussaïd M, Kapadia M, Thrash T, Sumner RW, Gross M, Helbing D, et al. Crowd behaviour during high-stress evacuations in an immersive virtual environment. *J R Soc Interface* 2016;13(122):20160414. <http://dx.doi.org/10.1098/rsif.2016.0414>.
- [29] Ioannou CC, Laskowski KL. A multi-scale review of the dynamics of collective behaviour: from rapid responses to ontogeny and evolution. *Phil Trans R Soc B* 2023;378(1874). <http://dx.doi.org/10.1098/rstb.2022.0059>.

- [30] Nagy M, Ákos Z, Biro D, Vicsek T. Hierarchical group dynamics in pigeon flocks. *Nature* 2010;464(7290):890–3. <http://dx.doi.org/10.1038/nature08891>.
- [31] Sosna MMG, Twomey CR, Bak-Coleman J, Poel W, Daniels BC, Romanczuk P, et al. Individual and collective encoding of risk in animal groups. *Proc Natl Acad Sci* 2019;116(41):20556–61. <http://dx.doi.org/10.1073/pnas.1905585116>.
- [32] Levis D, Diaz-Guilera A, Pagonabarraga I, Starnini M. Flocking-enhanced social contagion. *Phys Rev Res* 2020;2(3):032056. <http://dx.doi.org/10.1103/physrevresearch.2.032056>.
- [33] Poel W, Daniels BC, Sosna MMG, Twomey CR, Leblanc SP, Couzin ID, et al. Subcritical escape waves in schooling fish. *Sci Adv* 2022;8(25). <http://dx.doi.org/10.1126/sciadv.abm6385>.
- [34] Wu W, Zheng X, Romanczuk P. Escape cascades as a behavioral contagion process with adaptive network dynamics. *Phys Rev Res* 2025;7(1):013300. <http://dx.doi.org/10.1103/physrevresearch.7.013300>.
- [35] Liu Z, Liu T, Ma M, Hsu H, Ni Z, Chai Y. A perception-based emotion contagion model in crowd emergent evacuation simulation. *Comput Animat Virtual Worlds* 2018;29(3–4). <http://dx.doi.org/10.1002/cav.1817>.
- [36] Liu T, Liu Z, Chai Y, Wang J, Lin X, Huang P. Simulating evacuation crowd with emotion and personality. *Artif Life Robot* 2018;24(1):59–67. <http://dx.doi.org/10.1007/s10015-018-0459-5>.
- [37] Cao M, Zhang G, Wang M, Lu D, Liu H. A method of emotion contagion for crowd evacuation. *Phys A* 2017;483:250–8. <http://dx.doi.org/10.1016/j.physa.2017.04.137>.
- [38] Xu M, Xie X, Lv P, Niu J, Wang H, Li C, et al. Crowd behavior simulation with emotional contagion in unexpected multihazard situations. *IEEE Trans Syst Man Cybern: Syst* 2019;1–15. <http://dx.doi.org/10.1109/tsmc.2019.2899047>.
- [39] Xu M, Li C, Lv P, Chen W, Deng Z, Zhou B, et al. Emotion-based crowd simulation model based on physical strength consumption for emergency scenarios. *IEEE Trans Intell Transp Syst* 2021;22(11):6977–91. <http://dx.doi.org/10.1109/tits.2020.3000607>.
- [40] Ren J, Mao Z, Gong M, Zuo S. Modified social force model considering emotional contagion for crowd evacuation simulation. *Int J Disaster Risk Reduct* 2023;96:103902. <http://dx.doi.org/10.1016/j.ijdr.2023.103902>.
- [41] Mao Y, Yang S, Li Z, Li Y. Personality trait and group emotion contagion based crowd simulation for emergency evacuation. *Multimedia Tools Appl* 2018;79(5–6):3077–104. <http://dx.doi.org/10.1007/s11042-018-6069-3>.
- [42] Rincon J, Costa A, Villarrubia G, Julian V, Carrascosa C. Introducing dynamism in emotional agent societies. *Neurocomputing* 2018;272:27–39. <http://dx.doi.org/10.1016/j.neucom.2017.03.091>.
- [43] Yi W, Wu W, Wang X, Zheng X. Phase transitions in pedestrian evacuation: A dynamic modeling with small-world networks. *IEEE Trans Intell Transp Syst* 2024;25(11):18025–37. <http://dx.doi.org/10.1109/tits.2024.3433420>.
- [44] Dodds PS, Watts DJ. Universal behavior in a generalized model of contagion. *Phys Rev Lett* 2004;92(21):218701. <http://dx.doi.org/10.1103/physrevlett.92.218701>.
- [45] Wirth TD, Dachner GC, Rio KW, Warren WH. Is the neighborhood of interaction in human crowds metric, topological, or visual? In: Borge-Holthoefer J, editor. *PNAS Nexus* 2023;2(5). <http://dx.doi.org/10.1093/pnasnexus/pgad118>.
- [46] Feliciani C, Nishinari K. Measurement of congestion and intrinsic risk in pedestrian crowds. *Transp Res Part C: Emerg Technol* 2018;91:124–55. <http://dx.doi.org/10.1016/j.trc.2018.03.027>.
- [47] Moussaïd M, Helbing D, Theraulaz G. How simple rules determine pedestrian behavior and crowd disasters. *Proc Natl Acad Sci* 2011;108(17):6884–8. <http://dx.doi.org/10.1073/pnas.1016507108>.
- [48] Aldahlawi RY, Akbari V, Lawson G. A systematic review of methodologies for human behavior modelling and routing optimization in large-scale evacuation planning. *Int J Disaster Risk Reduct* 2024;110:104638. <http://dx.doi.org/10.1016/j.ijdrr.2024.104638>.
- [49] Yang Y, Xie D-F, Zhao X-M, Jia B. Two-stage stochastic optimization of passenger evacuation routes in metro stations considering stampede incidents. *Reliab Eng Syst Saf* 2025;260:111047. <http://dx.doi.org/10.1016/j.ress.2025.111047>.
- [50] Zhang Z, Jia L, Qin Y. Optimal number and location planning of evacuation signage in public space. *Saf Sci* 2017;91:132–47. <http://dx.doi.org/10.1016/j.ssci.2016.07.021>.
- [51] Skjermo J, Moscoso C, Nilsson D, Frantzich H, Hoem ÅS, Arnesen P, et al. Analysis of visual and acoustic measures for self-evacuations in road tunnels using virtual reality. *Fire Saf J* 2024;148:104224. <http://dx.doi.org/10.1016/j.firesaf.2024.104224>.
- [52] Zhang K, Chermprayong P, Xiao F, Tzoumanikas D, Dams B, Kay S, et al. Aerial additive manufacturing with multiple autonomous robots. *Nature* 2022;609(7928):709–17. <http://dx.doi.org/10.1038/s41586-022-04988-4>.
- [53] Hossain M. Autonomous delivery robots: A literature review. *IEEE Eng Manag Rev* 2023;51(4):77–89. <http://dx.doi.org/10.1109/emr.2023.3304848>.
- [54] Dorigo M, Theraulaz G, Trianni V. Swarm robotics: Past, present, and future [Point of View]. *Proc IEEE* 2021;109(7):1152–65. <http://dx.doi.org/10.1109/jproc.2021.3072740>.